Cellulose (2024) 31:2975–2988
https://doi.org/10.1007/s10570-024-05789-w

ORIGINAL RESEARCH

3D printed anti-swelling hydrogel scaffold with dialdehyde cellulose nanocrystals

Wei-Ting Ke · Der-Yun Cheng · I-Feng Wu · Ying-Chih Liao

Received: 10 May 2023 / Accepted: 1 February 2024 / Published online: 23 February 2024

Abstract In this study, a novel hydrogel preparation method was developed to formulate a 3D printable hydrogel with low swelling ratio for biomedical scaffolds. Nanocellulose fibrils were first oxidized to synthesize dialdehyde cellulose nanocrystals (DACs). The aldehyde groups on DACs could crosslink with laponite nanoclay via an esterification reaction. The mechanism between the two materials through aldehyde and hydroxyl groups was further confirmed by FTIR results. To optimize the printability and printing quality of the prepared hydrogels, the rheological properties of the gels were carefully examined to understand the shear thinning effect and the thixotropic responses. An optimal hydrogel composition of 6 wt% laponite and 1 wt% DACs showed the best results to accurately print 3D structures with a nozzle dispenser. The printed gel structures exhibited high mechanical strength and low swelling effect without complicated post treatment steps. Several examples were also demonstrated to show the structural stability, accuracy, and cell viability of the printed hydrogel structures for potential in 3D bio-printing applications.

Keywords 3D printable hydrogel · Anti-swelling · Dialdehyde cellulose nanocrystal · Laponite · Nanoclay · Biomedical scaffold

W.-T. Ke · D.-Y. Cheng · I.-F. Wu · Y.-C. Liao (✉)
Department of Chemical Engineering, National Taiwan University, Taipei 10617, Taiwan
e-mail: liaoy@ntu.edu.tw

W.-T. Ke
e-mail: r07524084@ntu.edu.tw

D.-Y. Cheng
e-mail: r10524057@ntu.edu.tw

I.-F. Wu
e-mail: r07524055@ntu.edu.tw

Y.-C. Liao
Advanced Research Center of Green Materials Science and Technology, College of Engineering, National Taiwan University, Taipei 10617, Taiwan

Introduction

In recent years, 3D bio-printing has attracted widespread attention in the field of tissue engineering, and has been extensively used to fabricate 3D biomedical scaffolds for organ and tissue regeneration (Ozbolat and Yu 2013; Chimene et al. 2016; Donderwinkel et al. 2017; Jang et al. 2018; Mobaraki et al. 2020). To achieve the printing accuracy and mechanical strength requirements in these 3D bio-printing applications, the bio-ink properties and material selection play a pivotal role. Specific features, such as viscoelasticity, rapid thixotropy, and resistance to swelling, are crucial factors in bio-ink formulation. Additionally, the bio-inks must be biocompatible for further biomedical applications. Among various biomaterials, hydrogels are often the preferred choice for 3D printing

bio-inks due to their high biocompatibility and biodegradability. However, many conventional bio-gels, such as alginate, collagen, hyaluronic acid, and gelatin, usually exhibit high fluidity but lack the necessary self-supporting property for effective use in 3D bio-printing (Gopinathan and Noh 2018). To enhance the mechanical strength, chemical treatments are commonly used to modify hydrogels for 3D bio-printing. However, these chemical approaches often compromise printability and may potentially affect cell viability (Guvendiren et al. 2016; Hospodiuk et al. 2017; Li et al. 2018).

To address the limitations of bio-gels, the introduction of nanoclay or other nanoparticle fillers into hydrogels has been proposed to enhance their rheological properties. Among these nanomaterials, laponite, a hydrous sodium lithium magnesium silicate with disc-shape particles, which has a dimension of ~ 25 nm in diameter and 1 nm in thickness, is widely employed in hydrogel composites due to its excellent intrinsic properties (Jin et al. 2017b). With negative charges on the plate surface and positive charges on the disk edge, laponite readily disperses in water. Moreover, laponite can self-assemble through electrostatic adsorption to form stable house-of-cards 3D nanostructures, which help impart high viscosity, pronounced thixotropic responses, and high shear-thinning behavior to the hydrogel composites. Thus, laponite can be regarded as a thickening agent for printing fluids to significantly improve the printability and structural stability of hydrogels (Jin et al. 2017a, 2017b). Besides its rheological benefits, recent research also indicates that laponite also reduces the degradation rate of hydrogel, enhancing their potential usage in composite hydrogels for 3D bio-printing applications (Golafshan et al. 2017). Furthermore, the abundant surface charges on laponite impart antimicrobial properties and provide sites for cell adhesion (Jang et al. 2018). Therefore, laponite has been identified as a highly promising filler for hydrogel composites, particularly in the context of 3D bio-printing.

However, despite the aforementioned advantages, laponite is seldom employed as the primary component in 3D bio-printing due to the limited mechanical properties (Chimene et al. 2016; Jang et al. 2018). One issue is that the physical electrostatic interaction between laponite disks is insufficient to provide necessary mechanical strength for printed structures using laponite hydrogels. Moreover, laponite hydrogels are prone to swelling when exposed to water, resulting in significant structural deformations (Chimene et al. 2016). Therefore, chemical modifications are commonly applied to nanoclay materials to enhance the mechanical strength of their hydrogel composites and to prevent swelling of the printed structure. For example, Zhang et al. (2019) successfully crosslinked polyvinyl alcohol and montmorillonite with glutaraldehyde, greatly improving the mechanical strength of composite films. However, it is worth noting that commercial aldehyde crosslinkers such as formaldehyde or glutaraldehyde usually possess biological toxicity, limiting their uses in the biomedical field. Cellulose nanocrystals (CNCs), as an environmentally friendly material derived from plants, have gained attention due to their high biocompatibility, and featuring abundant surface hydroxyl groups suitable for additional surface treatments. To enhance their reactivity with laponite, CNCs can be surface-modified into dialdehyde cellulose nanocrystals (DACs). DAC, equipped with the dialdehyde surface groups, has been widely used as a crosslinker in cell culture mediums, such as gelatin (Jiang et al. 2018), effectively enhancing the mechanical properties of hydrogel scaffolds. Following a similar mechanism, DAC nano-sticks can firmly crosslink with laponites to improve the rheological performances of the modified hydrogels for 3D bio-printing. Furthermore, the high crystallinity of DACs can also stabilize the hydrogel structure (Huang et al. 2019), resulting in increased mechanical strengths and reduced swelling ratio, thereby promoting the stability of the printed structures.

In this research, a novel hydrogel synthesis method is proposed to prepare 3D printed hydrogel structures with a low swelling ratio. DACs are first synthesized by mild oxidation of CNCs to serve as biocompatible aldehyde crosslinkers with low cytotoxicity. A hydrogel composite made by DACs and laponite is then formulated to optimize the rheological properties for extrusion 3D printing. The structural fidelity, mechanical strength and anti-swelling behavior are shown to be largely improved while maintaining printability through chemical crosslinking mechanism between DACs and laponite at optimum hydrogel formulation conditions. Finally, complex 3D structures are printed and cell viability tests are examined to demonstrate the potential application of this novel bio-ink for biomedical applications.

Materials and methods

Materials preparation

Sodium periodate 98% was purchased from Alfa Aesar, USA. Laponite RD was purchased from BYK additives, USA, having a disc-shaped structure with a diameter of 25 nm and a thickness of 1 nm. Cellulose nanocrystals (CNCs) were provided by the University of Maine. Ethylene glycol 99.8%, sodium hydroxide 98% pellets, bromophenol blue, calcein AM 96.0%, and ethidium homodimer-1 90% were all purchased from Sigma-Aldrich, USA. Hydrogen chloride (36%) and phosphate-buffer saline (pH 7.4) were acquired from Kanto Chemical, Japan, and Uni-Region, Taiwan, respectively. Dulbecco's Modified Eagles Medium–High Glucose (SH30003.02) containing mouse fibroblast L929 was provided by Hyclone, USA. Fetal Bovine Serum (420,201) was purchased from Biolegend, USA. AlamarBlue was purchased from ThermoFisher, USA. PSA antibiotic agent was purchased from BioVision, Switzerland. All chemicals were used as received without further purification.

Synthesis of dialdehyde cellulose nanocrystals (DACs)

The procedure is depicted in Fig. 1 (Larsson et al. 2013; Sun et al. 2015; Yao et al. 2016). First, 40 g of 12.1 wt% CNC aqueous solution was diluted into a 100 g solution with DI water. Then, 14.5 g of sodium periodate was dissolved in a flask of 50 mL of water and the solution was heated up to 50 °C. The two as-prepared solutions were stirred by a magnetic stirrer and kept at room temperature for 2 h. It should be noted that the reaction should be kept away from light. After the reaction, 2 mL of ethylene glycol was added and the solution stirred at room temperature for 30 min to terminate the reaction. The mixture was then centrifuged at 10,000 rpm for 15 min and the white precipitations were collected into a dialysis bag (Cellu-Sep, Nominal MWCO: 12,000–14,000). The samples were dialyzed for one week and the water was refreshed once a day until the conductivities of liquids between both sides of the bag became the same. At last, the product was dispersed in water by the ultrasonic homogenizer (Omni, Ruptor 4000) and preserved under 4°C.

Identification of degree of oxidation of DACs

Cannizzaro method was used to examine the degree of oxidation. After 0.1 g of DAC powder was dispersed in 5 mL of 0.05 M sodium hydroxide by ultrasonic homogenizer, the solution was heated at 70 °C for 10 min then cooled down to room temperature. To provide excessive acid, 6 mL of 0.05 M hydrogen chloride was added to the mixture. A few drops of Bromophenol Blue were then added as the pH indicator. The standard solution, 0.01 M of sodium hydroxide, was applied to the back titration. When the color of the solution changed from yellow to blue, the titration was halted and the volume of the standard solution used was recorded. The degree of oxidation (DO) of DACs can be calculated with the following equation:

$$\mathrm{DO} = \frac{(0.01\mathrm{V} + 0.05 \times 5 - 0.05 \times 6) \times 10^{-3}}{0.1/160}$$

where V is the volume of the standard sodium hydroxide solution consumed by back titration method (Yao et al. 2016).

Characterization

The rheological properties of the hydrogels including viscosity, storage and loss modulus, yield stress, and thixotropy were measured by a rheometer (Discovery HR-2, TA Instruments, USA), which was equipped with a cone-plate with a diameter of 40 mm and a cone angle of 3.5949°. The viscosities of samples were measured at shear rates ranging from 0.01 to 350 s^{-1}. The modulus was measured between angular frequencies of 0.06 and 60 rad/s. Yield stresses were measured with the oscillation strain increasing from 0.1 to 1000% using amplitude sweep method, and the angular frequency was controlled constantly at 6.28 rad/s. All measurements were performed at 25°C. Nanocellulose samples were first freeze dried into powder form without milling. The powder samples were then deposited on copper grids (200 mesh, coated with silicon monoxide). Transmission electron microscopy (TEM, JEOL, JEM-2100F, Japan) was used to analyze the size and shape of prepared TEM samples at an accelerating voltage of 200 kV. The Fourier-transform infrared spectroscopy was

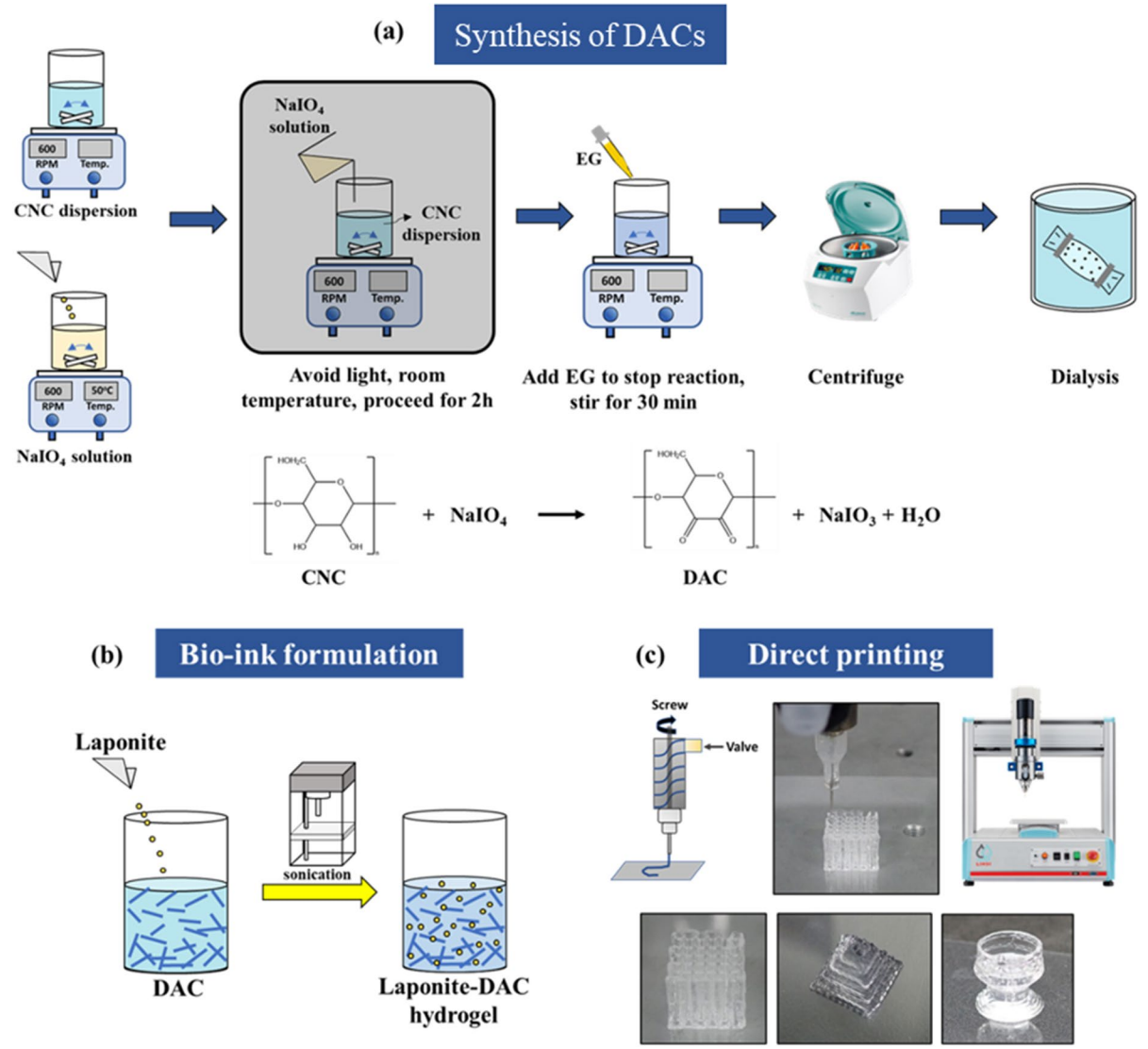

Fig. 1 **a** Schematic illustration of the synthesis of dialdehyde cellulose nanocrystals (French 2017), **b** bio-ink formulation and **c** 3D printing process

obtained with a spectrometer (Spectrum 100, Perkin Elmer). X-ray Diffractometer (XRD; SmartLab SE, Rigaku, The Woodlands, Texas, USA) with a Cu Kα radiation (wavelength of 1.5406 Å) was used to confirm the powder composition and crystallinity. A scan ranging from 10° to 90° was used with a scan rate of 3°/min and 0.05° scan step. The compression test was conducted with the aforementioned rheometer to evaluate the relationship between stress and strain. The compressive Young's modulus of different gel compositions was calculated based on the slope during the initial 5% of deformation. The measurements of each property test were based on at least three tests, and the average values were shown in the graphs.

Laponite/DAC gel for 3D structures

First, 20 mL DAC solutions of different concentrations (0 wt%, 0.5 wt%, 1 wt%, 1.5 wt%, and 2 wt%) were prepared and adjusted to pH 3 by addition of 0.1 M hydrogen chloride. Afterwards, a

proper proportion (0 wt%, 1 wt%, 2 wt%, 3 wt%, 4 wt%, 5 wt%, or 6 wt%) of laponite powder was added into the DAC samples. An ultrasonic homogenizer was used to disperse the powder until the mixture became translucent. The prepared gels were further de-aerated with planetary centrifugal mixer (ARE-310, THINKY, USA), and stored at 4 °C before printing. The 3D structures were printed on a PET substrate by an automatic dispenser (LH-400w, Lishi Technology, Taiwan) with a 23G needle (600 μm inside diameter). The 3D printing process was proceeded at room temperature with a back pressure of 25 psi, printing speed of 10 mm/s, and a nozzle-substrate gap distance of 0.2 mm.

Cell adhesion and viability tests

A solid cylinder with approximately a 1.5-cm diameter and a 0.5-mm thickness was printed and exposed under ultraviolet light to sterilize. About 10 mL of DMEM medium was dripped into the well, which was consisted of 10% of fetal bovine serum (FBS) and 1% of PSA antibiotic agent. The gel ink was then immersed in the cultivation medium for 30 min. Then, 2 mL of trypsin EDTA was added to prevent cells from attaching on the dish. The cells were seeded onto the medium with a concentration of 15,000/well. After 24 and 96 h, cultivation media were removed and washed with phosphate buffered saline (PBS) twice. Then, the printed gel structure was immersed into PBS solution with 10.0 μg/mL of calcein AM and 10.0 μg/mL of ethidium homodimer-1. The sample was kept still for five minutes at room temperature in the dark. AlamarBlue was used to dye in the cell viability test. The status of the growth and death of cells was observed via a fluorescence microscope.

Result and discussion

Characterization of DAC

The prepared DAC powder is first examined via FTIR spectra to confirm the existence of aldehyde on DACs. As shown in Fig. 2a, a shoulder peak of aldehyde appears at wavenumber of 1735 cm^{-1}, which refers to the successful surface modification of CNCs. To further confirm the chemical modification, Tollen's test is also performed to support this result. As shown in the inset picture of Fig. 2b, after the addition of Tollen's agent, the solution color becomes yellow, indicating nano-silver recovery by the aldehyde groups on DACs. Furthermore, for the synthesized DAC solution, the titration results based on Cannizzaro method (Yao et al. 2016) show a DO value of 0.27, representing that there is one aldehyde group within every 4 monomer units. The structure and crystallinity of the cellular nanofibers before and after reaction are also investigated. The XRD results (Fig. 2b) show two distinct peaks at 16.5 and 22.5 degrees, indicating the (1 1 0) and (2 0 0) planes, respectively (Gong et al. 2017). But the lower peak values of DAC samples indicate slight decrease in crystallinity after the ring cleavage reaction with $NaIO_4$. Yet, from TEM analyses (Fig. 2c), the DACs still remain similar stick-shaped structures as the pristine CNCs but with few broken cellulose residues, indicating that no large crystalline fractures after surface modification.

To understand the crosslinking mechanism between laponite and DAC, the FTIR spectra of pristine laponite and laponite/DAC hydrogel after air-drying are compared in Fig. 2d. For the laponite/DAC sample, an additional peak at wavenumber of 1120 cm^{-1} indicates the formation of Si–O–C bond after crosslinking. Therefore, laponite and DAC are indeed able to crosslink through aldehyde group as the scheme in Fig. 2e.

Optimization of hydrogel printability

To optimize the rheology and printability of the hydrogel, the concentrations of DACs and laponite in the hydrogel are adjusted. To evaluate the printability of the prepared gels during the extrusion through the dispenser, the relation between viscosity and shear rate is first investigated. As shown in Fig. 3a, the laponite gels have a shear-thinning behavior and the gel viscosity increases as laponite concentration increases. Moreover, the hydrogels become nearly solid and can resist gravity (inset picture in Fig. 3c). The viscoelasticity of the laponite hydrogels is also measured to understand the rheological changes with high laponite loading (Fig. 3b). It is found that storage modulus G′ is always larger than the loss modulus G″ for all laponite gels, indicating gelling behavior due to the strong interaction between laponite particles. The tan δ value (Fig. 3c), or the

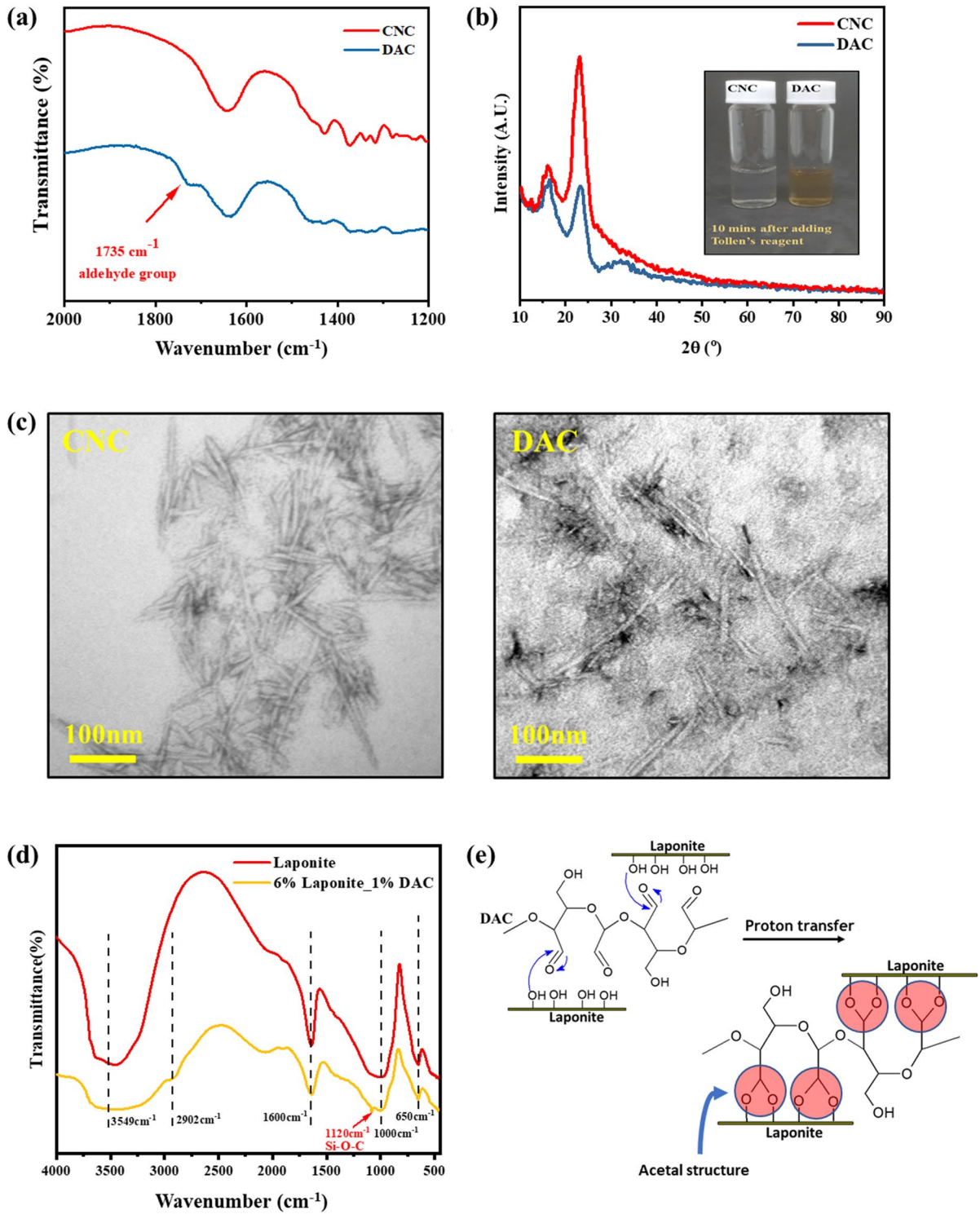

Fig. 2 **a** FTIR spectra of CNC and DAC powders. **b** XRD patterns of CNCs and DACs, showing the crystallinity of DACs slightly decreases after the ring cleavage reaction with $NaIO_4$. **c** TEM images of CNCs and DACs, showing that the CNCs remain their rod-shaped structures after converted into DACs. **d** FTIR spectra of laponite and laponite/DAC hydrogels. **e** Schematic diagram of the proposed crosslinking mechanism between laponite nanoclay and DAC

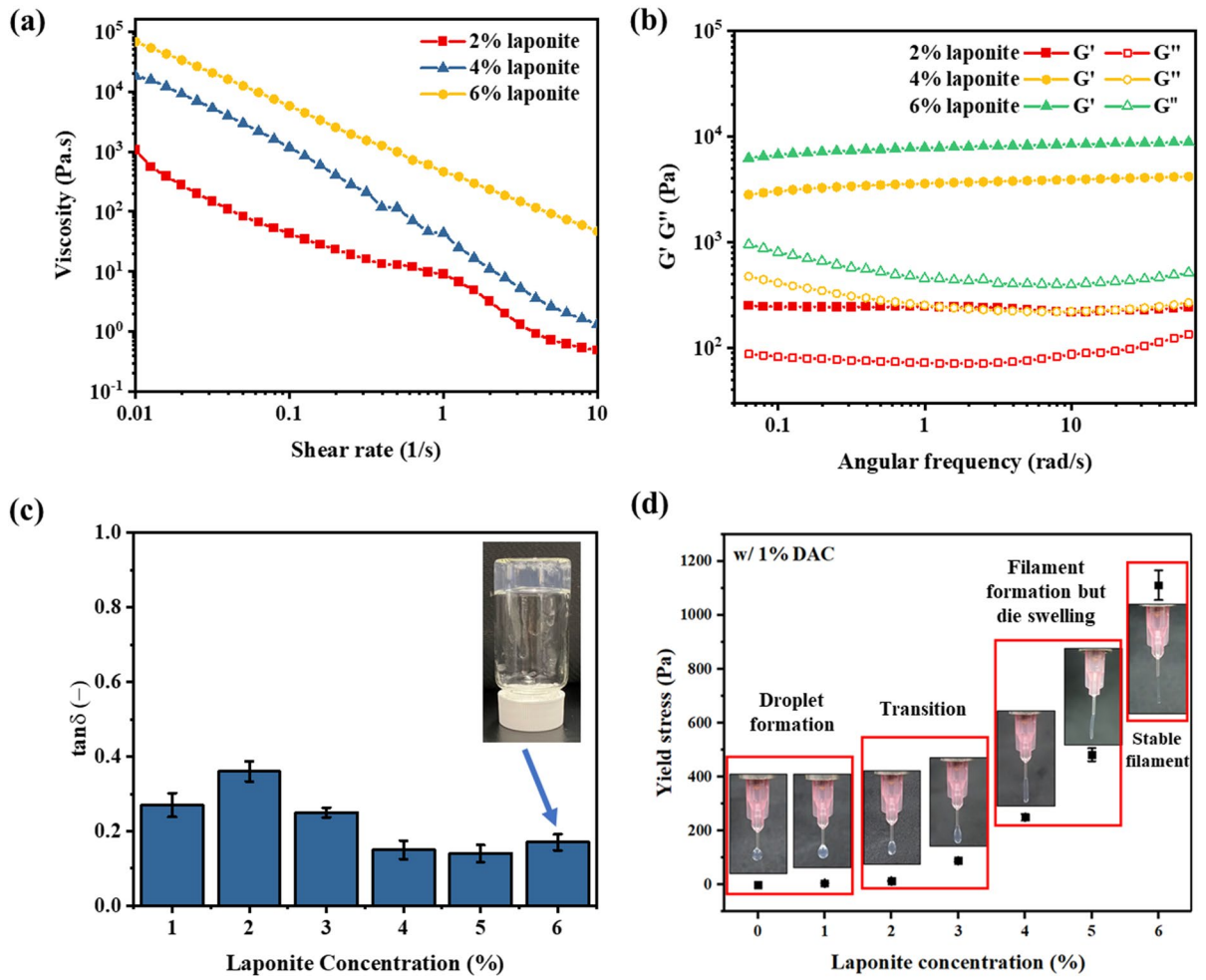

Fig. 3 **a** Variation of viscosity with shear rate. **b** The storage (G′) and loss modulus (G″) of laponite hydrogels. **c** The tan δ values of hydrogel samples at an angular frequency of 0.1 rad/s. **d** Effects of yield stress on hydrogel extrusion behavior. The error bars in (c) and (d) indicate the standard deviation of the measurements

ratio between G″ and G′, is always less than unity for these samples, indicating their gel nature. However, due to the low viscosity at high shear rates, as shown in Fig. 3d, strong surface tension force dominates the extrusion process (Du et al. 2018), and thus the extruded hydrogels form droplets at low laponite concentrations. Thus, it is difficult to draw continuous filaments for 3D object formation. To enhance the printability of the hydrogels, i.e. to form stable and continuous cylindrical filaments, yield stress of the hydrogel needs to be increased to resist the surface tension (Duty et al. 2018). As laponite concentration increases to 4 wt%, the increase in yield stress helps the extruded hydrogel stay intact as a cylindrical filament without deformation by surface tension forces. However, an increase in filament diameter after extrusion, or so-called die swelling phenomenon, is observed (Grosskopf et al. 2018). The die swelling phenomenon leads to unstable diameter in the printing process and thus degrades the printing quality. To eliminate the die swelling phenomenon, the yield stress of hydrogel is further increased by increasing laponite contents (Grosskopf et al. 2018), so that a straight extruded filament with consistent radius close to the needle can be obtained for better printability (Jin et al. 2017a). From the experiments, at least 6 wt% laponite is needed to provide sufficient yield stress for stable filament in the printing process.

Thus, for experiments in the following sections, the concentration of laponite is fixed at 6 wt% to find the optimal DAC ratio for 3D printing.

Besides laponite concentration adjustments, the addition of stick-shaped DACs can further strengthen the rheological properties of hydrogels for better printability (Rutz et al. 2015). As shown in Fig. 4a, as the DAC concentration increases, the loss modulus (G″) of the hydrogel elevates phenomenally while the storage modulus (G′) remains constant. This indicates that the fluidity of the hydrogel enhances with higher DAC content (Fig. 4b). When the gel is extruded through the nozzle, the stick-shaped laponite nanoparticles are forced to re-arrange their orientations to comply with the imposed shear stress (Hausmann et al. 2018). Therefore, in addition to shear thinning and viscoelastic behavior, thixotropy also plays an important role for hydrogel solidification in 3D extrusion printing (Gao et al. 2018; Dávila and d'Ávila 2019). When the viscoelastic hydrogel is extruded from the nozzle tip, it experiences a sudden change in shear rates, and results in a time-dependent viscosity. To evaluate the thixotropic properties of the hydrogels, a sudden shear rate elevation from 0.1 to 300 s^{-1} is performed. As shown in Fig. 4c, the viscosity hydrogels can reach equilibrium values within 2 s, indicating fast thixotropic response of the hydrogel. The viscosity ratio between the lowest and highest shear rates, or thixotropic index (TI), however, shows the differences in the printability. Without DACs, the

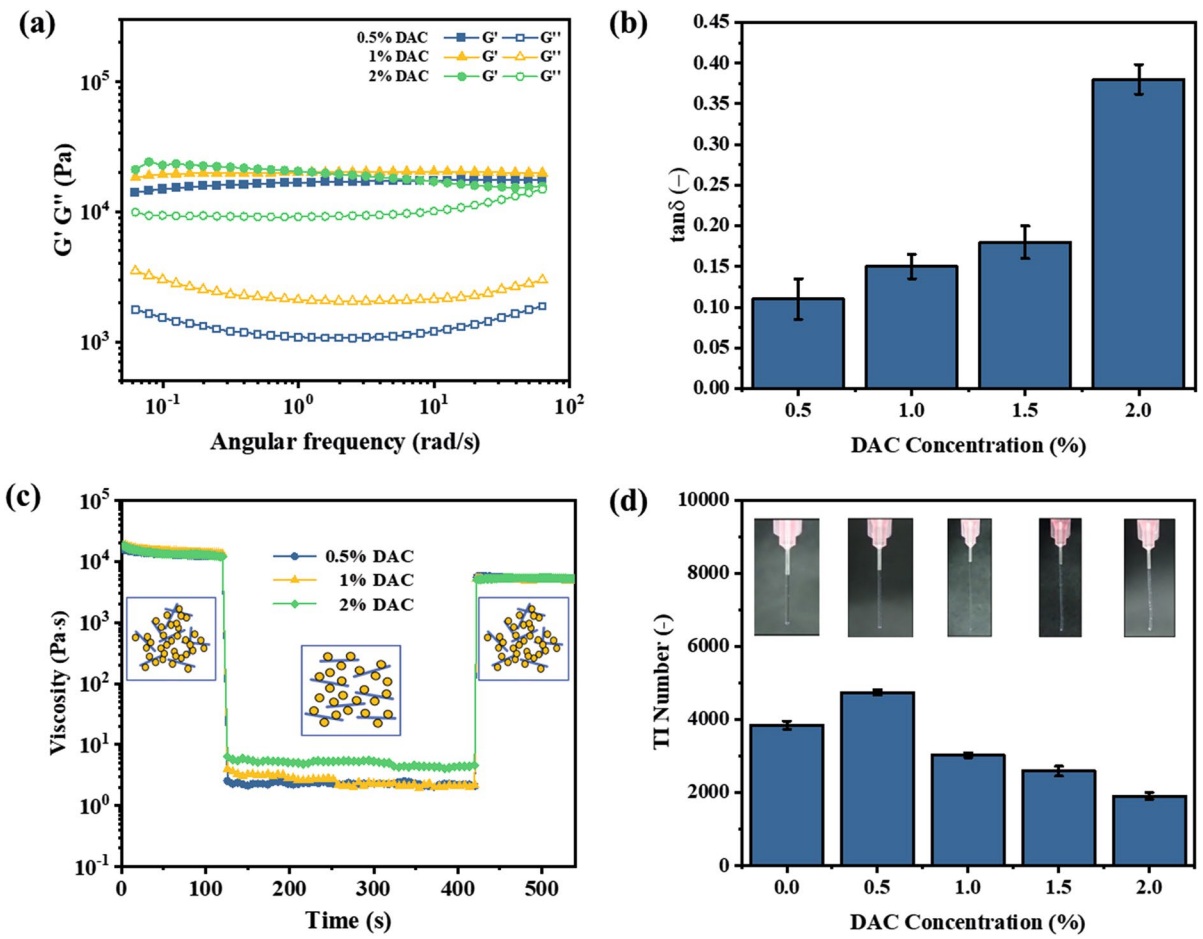

Fig. 4 **a** Variation in dynamic modulus with shear rate. **b** Variation in tan δ values with DAC concentrations at an angular frequency of 0.1 rad/s. **c** Thixotropic responses of hydrogels with different DAC concentrations. **d** Effects of thixotropic index on hydrogel extrusion behavior. The samples used here are composed of various DAC concentration (0–2 wt%) with 6 wt% laponite. The error bars in (b) and (d) indicate the standard deviation of the measurements

filament has a slight die swelling phenomenon due to the low TI value. At 0.5 wt% and 1 wt% DACs, a stable filament with smooth surface is formed due to its high TI thixotropic properties and therefore can result in better printing precision (Jin et al. 2017a). When the DAC concentration is more than 0.5 wt%, the excessive DACs suppress the viscosity decrease at high shear rates. Thus, the TI value decreases and the extruded filament becomes unstable, resulting in lower printing quality (Kuo et al. 2019).

Mechanical properties

The printed hydrogel structures show good mechanical strength with large compressive supporting capacity. For 3D printed structures, the bottom layers need to bear the weight of upper layers to prevent collapse in the printing process (Sun et al. 2018). To evaluate the mechanical strength of 3D printed hydrogel, a 1 cm^3 cube is fabricated with the 3D printing dispenser. A compression test is then conducted with a rheometer to obtain the compressive Young's modulus and strength of different hydrogel compositions. As shown in Fig. 5a, the compressive stress is strengthened after DAC addition due to the crosslinking between DACs and laponite. The hydrogel with 1 wt% DACs shows the highest Young's modulus, which is about four times higher than the hydrogel without DACs. But when the DAC concentration exceeds 1 wt%, the mechanical strength starts to decrease because the excessive DAC-laponite crosslinking affects the electrostatic attraction between laponites and reduces the overall mechanical strength (Kuo et al. 2019). At the optimum hydrogel composition with 1 wt% DAC addition, the printed cube can withstand a 100 g

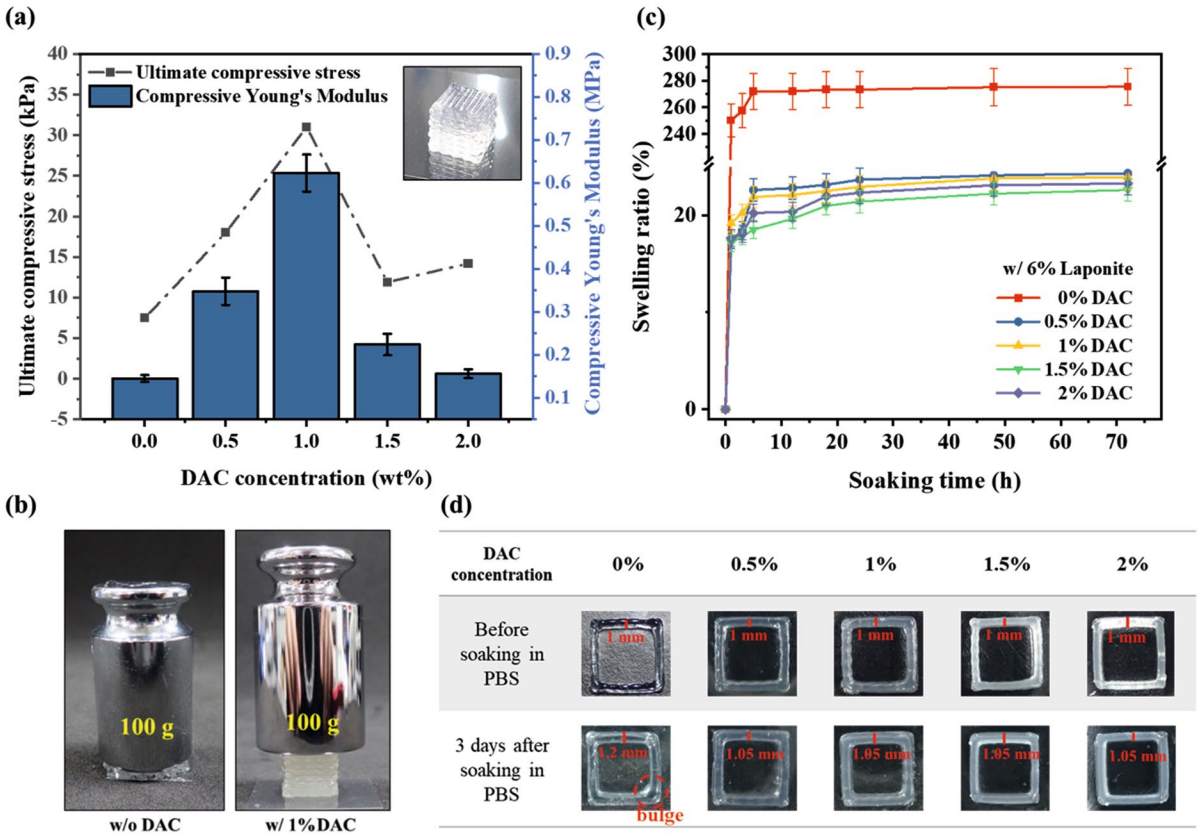

Fig. 5 **a** The compression test and compressive Young's modulus of different compositions of hydrogels. **b** Depiction of the mechanical strength of hydrogels. **c** The comparison of swelling ratio of each composition of gel ink along with its soaking time. **d** Pictures displaying the difference in swelling phenomenon of DAC concentration varying between 0 and 2 wt% with 6 wt% laponite. The error bars in the graph indicate the standard deviation of the measurements

weight (Fig. 5b), while the one with pristine laponite collapses directly.

Swelling behavior

The crosslinked DAC/laponite hydrogel also shows great shape stability. Generally, hydrogels swell after submerged in water-based cell culture media. This swelling behavior not only leads to large shape deformation but also weakens the mechanical strength. To measure the swelling properties of the DAC/laponite hydrogels, square wells with 1 cm side length (Fig. 5d) are printed and then submerged in phosphate buffer solution for swelling ratio examination. The swelling ratio is determined by comparing the weight variation between the structures before and after absorbing water (Holback et al. 2011). As shown in Fig. 5d, the swelling behavior of hydrogels can be well reduced by DAC addition: the walls remain nearly the same thickness after 3 days in aqueous PBS solution. To quantitatively evaluate the swelling behavior, (Ahlfeld et al. 2017) the transient variation of swelling ratio for printed hydrogel structures immersed in PBS is recorded for 3 days. Without DAC addition, the pristine laponite gel is constructed by electrostatic attractions and hydrogen bonds between laponite molecules, and can be easily damaged by water. Thus, pristine laponite hydrogel shows a higher swelling ratio up to 2.8 times after immersed in PBS. After adding DACs, the swelling ratio reduces to ~ 20% regardless of the DAC concentration. Moreover, no obvious deformation is observed and the shape can remain nearly the same. These evidences indicate that the chemical crosslinking between laponite and DACs can help restraining the phenomenon of swelling. Thus, considering both swelling and mechanical properties, the hydrogel with 1 wt% DACs and 6 wt% laponite will be used in the following sections.

Printed 3D structures

With the optimum composition for printability and stability, the hydrogel ink can be used to print complex 3D structures. A dispenser with an extruded filament of ~ 0.2 mm diameter is used. As shown in Fig. 6a, b, a pyramid and a goblet are printed. Compared with the original CAD design, the printed hydrogel pyramid has a bottom length of 1 cm after printing 25 layers of hydrogel. The length difference between every layer is only approximately 0.4 mm, showing good printing accuracy. Besides printing accuracy, the concave structure of the goblet can be printed without any supporting framework, indicating the strong mechanical strength of the hydrogel (Jin et al. 2017b). In addition, the printed goblet can be filled up with water without leaking, indicating that the layers attach well in between and the structure is able to withstand hydrostatic pressure without rupture. To further demonstrate the printing accuracy for complex geometry, an ear scaffold is printed through the robotic dispenser with a layer thickness of 0.2 mm. As shown in Fig. 6c, the printed samples exhibit excellent precision, accurately reproducing the designed details with deviations of less than 5%, which is in good agreement with the original CAD design.

Cell adhesion and viability

To evaluate the bio-compatibility of the DAC/laponite gel, cell viability tests are performed. After cultivation, the results are observed through an optical microscope (Fig. 7a). Mouse fibroblast L929 cells on the prepared gel layer show round and fusiform structures, indicating the inherent cell affinity and good cell adhesion (Bettinger et al. 2009) of the DAC/laponite gel. To further investigate the cell viability of the DAC/laponite hydrogel, Calcein AM and ethidium homodimer-1 are used as colorants for cell viability examination. As shown in Fig. 7c, d, the light green bands in the image show a vast amount of dyed living cells, and few dead cells are observed. This result implies that the hydrogel has high cell viability and is nontoxic to cells. In order to quantify cell physiological activity, AlamarBlue reduction identification is conducted. AlamarBlue colorant is initially dark blue without fluorescence and then turns pink when the reagent reacts with dehydrogenase NADH in mitochondria. By converting the fluorescence results to the reagent reduction rate, the physiological responses can be well interpreted. As shown in Fig. 7b, AlamarBlue reduction continuously increases after four days of cultivation. This increment indicates that the cells have reliable adhesion, growth and reproduction on the 3D bio-printing structure (Jakab et al. 2010; Rutz et al. 2017). These evidences show that the printed 3D structures can provide a good

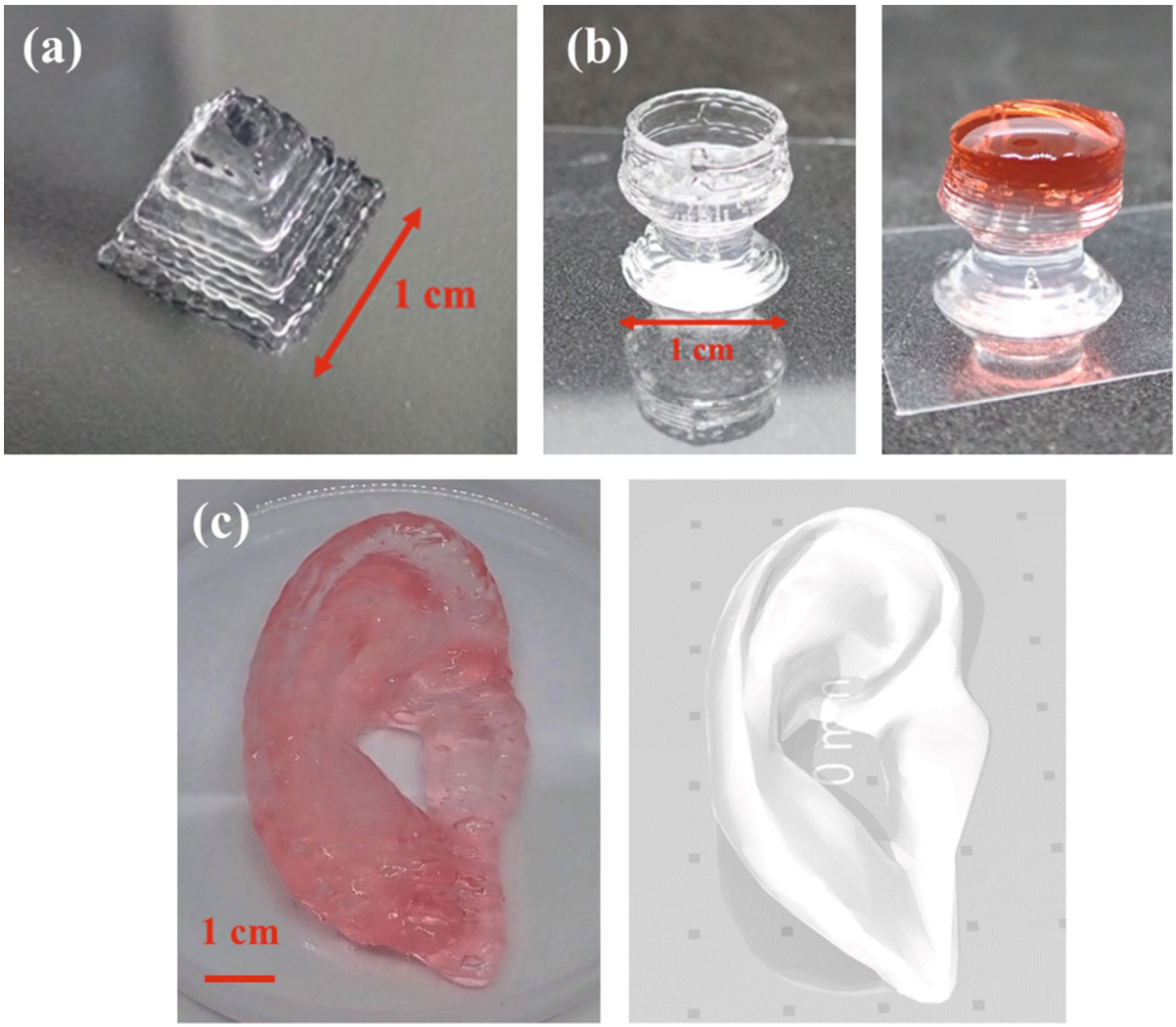

Fig. 6 **a** Printed pyramid structure with 25 layers and a bottom length of 1 cm. **b** Printed goblet filled with dyed liquid without leaking and swelling. **c** A printed hydrogel structure with an ear shape. The structure is dyed with Congo red. The original CAD design is displayed on the right for comparison

scaffold surface for cell growth and thus have a great potential for biomedical applications, such as artificial organs and bone tissue regeneration.

Conclusion

In this study, a new hydrogel formulation is developed to produce an anti-swelling gel 3D printed structures for biomedical scaffold. Nanocellulose fibrils are first oxidized to functionalize the surface with aldehyde groups. The functionalized cellulose exhibits strong interaction with laponite particles. The crosslinking mechanism between the two materials through aldehyde and hydroxyl groups is also confirmed by FTIR results. To optimize the printability and printing quality of the prepared hydrogels, the rheological properties of the hydrogels are carefully examined to understand the shear thinning effect and the thixotropic responses of the prepared gels. An optimal hydrogel composition of 6 wt% laponite and 1 wt% DACs shows the best results to accurately print 3D structures with a nozzle dispenser. The printed

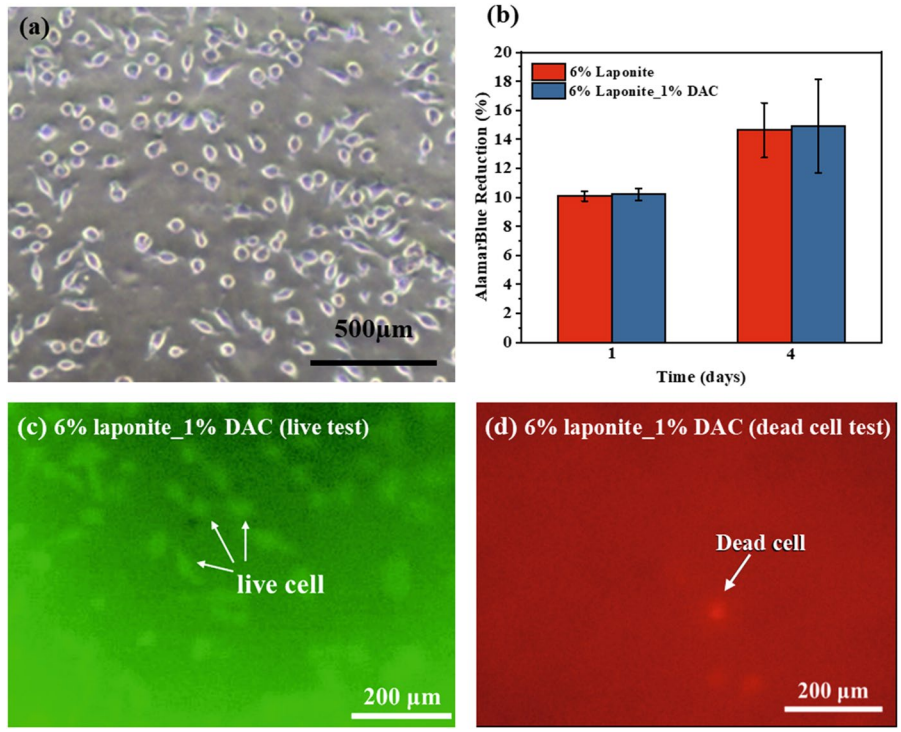

Fig. 7 **a** Microscopic image of L929 cells on printed hydrogel after four days of cultivation. **b** The quantitative results of cell viability via AlamarBlue reduction test. **c-d** The live and dead cell tests of the L929 cells on the printed hydrogel samples. The error bars in the graph indicate the standard deviation of the measurements

hydrogel structures show high mechanical strength and low swelling effect without complicated post-treatment steps. Several examples are also demonstrated to show the remarkable structural stability, accuracy, and cell viability of the printed gel structures. Overall, the hydrogel formulation in this study shows good potential in 3D bio-printing and can be further extended to print complex structures for organ regeneration and tissue culturing.

Acknowledgements This study is supported by the National Science and Technology Council in Taiwan (NSTC 112-2221-E-002-026 -MY3 and NSTC112-2622-E-002-035).

Authors' contributions YCL, WTK, and DYC wrote the main manuscript text. WTK, IFW, and DYC prepared figures. All authors reviewed the manuscript.

Funding This work is supported by National Science and Technology Council (NSTC 112-2221-E-002026 -MY3 and NSTC112-2622-E-002-035).

Data availability The results/data/figures in this manuscript have not been published elsewhere, nor are they under consideration by another publisher. All of the material is owned by the authors and/or no permissions are required.

Declarations

Conflict of interest The authors declare no competing interests.

Ethical approval Comply with ethical standards.

Consent for publication The manuscript has been approved for publication by all authors.

References

Ahlfeld T, Cidonio G, Kilian D, Duin S, Akkineni A, Dawson J, Yang S, Lode A, Oreffo R, Gelinsky M (2017) Development of a clay based bioink for 3D cell printing for skeletal application. Biofabrication 9:034103. https://doi.org/10.1088/1758-5090/aa7e96

Bettinger CJ, Langer R, Borenstein JT (2009) Engineering substrate topography at the micro-and nanoscale to control cell function. Angew Chem Int Ed 48:5406–5415. https://doi.org/10.1002/anie.200805179

Chimene D, Lennox KK, Kaunas RR, Gaharwar AK (2016) Advanced bioinks for 3D printing: a materials science perspective. Ann Biomed Eng 44:2090–2102. https://doi.org/10.1007/s10439-016-1638-y

Dávila JL, d'Ávila MA (2019) Rheological evaluation of Laponite/alginate inks for 3D extrusion-based printing.

Int J Adv Manuf Technol 101:675–686. https://doi.org/10.1007/s00170-018-2876-y
Donderwinkel I, Van Hest JC, Cameron NR (2017) Bio-inks for 3D bioprinting: recent advances and future prospects. Polym Chem 8:4451–4471. https://doi.org/10.1039/C7PY00826K
Du Z, Yu X, Han Y (2018) Inkjet printing of viscoelastic polymer inks. Chin Chem Lett 29:399–404. https://doi.org/10.1016/j.cclet.2017.09.031
Duty C et al (2018) What makes a material printable? A viscoelastic model for extrusion-based 3D printing of polymers. J Manuf Process 35:526–537. https://doi.org/10.1016/j.jmapro.2018.08.008
French AD (2017) Glucose, not cellobiose, is the repeating unit of cellulose and why that is important. Cellulose 24:4605–4609. https://doi.org/10.1007/s10570-017-1450-3
Gao T, Gillispie GJ, Copus JS, Pr AK, Seol Y-J, Atala A, Yoo JJ, Lee SJ (2018) Optimization of gelatin–alginate composite bioink printability using rheological parameters: a systematic approach. Biofabrication 10:034106. https://doi.org/10.1088/1758-5090/aacdc7
Golafshan N, Rezahasani R, Esfahani MT, Kharaziha M, Khorasani S (2017) Nanohybrid hydrogels of laponite: PVA-Alginate as a potential wound healing material. Carbohydr Polym 176:392–401. https://doi.org/10.1016/j.carbpol.2017.08.070
Gong J, Li J, Xu J, Xiang Z, Mo L (2017) Research on cellulose nanocrystals produced from cellulose sources with various polymorphs. RSC Adv 7:33486–33493. https://doi.org/10.1039/C7RA06222B
Gopinathan J, Noh I (2018) Recent trends in bioinks for 3D printing. Biomater Res 22:1–15. https://doi.org/10.1186/s40824-018-0122-1
Grosskopf AK, Truby RL, Kim H, Perazzo A, Lewis JA, Stone HA (2018) Viscoplastic matrix materials for embedded 3D printing. ACS Appl Mater Interfaces 10:23353–23361. https://doi.org/10.1021/acsami.7b19818
Guvendiren M, Molde J, Soares RM, Kohn JJAbs, engineering, (2016) Designing biomaterials for 3D printing. ACS Biomater Sci Eng 2:1679–1693. https://doi.org/10.1021/acsbiomaterials.6b00121
Hausmann MK et al (2018) Dynamics of cellulose nanocrystal alignment during 3D printing. ACS Nano 12:6926–6937. https://doi.org/10.1021/acsnano.8b02366
Holback H, Yeo Y, Park K (2011) Hydrogel swelling behavior and its biomedical applications. In: Biomedical hydrogels. Elsevier
Hospodiuk M et al (2017) The bioink: a comprehensive review on bioprintable materials. Biotechnol Adv 35:217–239. https://doi.org/10.1016/j.biotechadv.2016.12.006
Huang W, Wang Y, McMullen LM, McDermott MT, Deng H, Du Y, Chen L, Zhang L (2019) Stretchable, tough, self-recoverable, and cytocompatible chitosan/cellulose nanocrystals/polyacrylamide hybrid hydrogels. Carbohydr Polym 222:114977. https://doi.org/10.1016/j.carbpol.2019.114977
Jakab K, Norotte C, Marga F, Murphy K, Vunjak-Novakovic G, Forgacs G (2010) Tissue engineering by self-assembly and bio-printing of living cells. Biofabrication 2:022001. https://doi.org/10.1088/1758-5082/2/2/022001
Jang T-S, Jung H-D, Pan HM, Han WT, Chen S, Song J (2018) 3D printing of hydrogel composite systems: recent advances in technology for tissue engineering. Int J Bioprinting. https://doi.org/10.18063/ijb.v4i1.126
Jiang Y, Zhou J, Yang Z, Liu D, Xv X, Zhao G, Shi H, Zhang Q (2018) Dialdehyde cellulose nanocrystal/gelatin hydrogel optimized for 3D printing applications. J Mater Sci 53:11883–11900. https://doi.org/10.1007/s10853-018-2407-0
Jin Y, Chai W, Huang Y (2017a) Printability study of hydrogel solution extrusion in nanoclay yield-stress bath during printing-then-gelation biofabrication. Mater Sci Eng C 80:313–325. https://doi.org/10.1016/j.msec.2017.05.144
Jin Y, Liu C, Chai W, Compaan A, Huang Y (2017b) Self-supporting nanoclay as internal scaffold material for direct printing of soft hydrogel composite structures in air. ACS Appl Mater Interfaces 9:17456–17465. https://doi.org/10.1021/acsami.7b03613
Kuo C, Qin H, Acuña D, Cheng Y, Jiang X, Shi X (2019) Printability of hydrogel composites using extrusion-based 3D printing and post-processing with calcium chloride. J Food Sci Nutr 5:051. https://doi.org/10.24966/FSN-1076/100051
Larsson PA, Kochumalayil JJ, Wågberg L (2013) Oxygen and water vapour barrier films with low moisture sensitivity fabricated from self-cross-linking fibrillated cellulose. In 15th fundamental research symposium: advances in pulp and paper research, pp 851–866. The Pulp and Paper Fundamental Research Society Cambridge, UK
Li H et al (2018) Review of 3D printable hydrogels and constructs. Mater Des 159:20–38. https://doi.org/10.1016/j.matdes.2018.08.023
Mobaraki M, Ghaffari M, Yazdanpanah A, Luo Y, Mills D (2020) Bioinks and bioprinting: a focused review. Bioprinting 18:e00080. https://doi.org/10.1016/j.bprint.2020.e00080
Ozbolat IT, Yu Y (2013) Bioprinting toward organ fabrication: challenges and future trends. IEEE Trans Biomed Eng 60:691–699. https://doi.org/10.1109/TBME.2013.2243912
Rutz AL, Hyland KE, Jakus AE, Burghardt WR, Shah RN (2015) A multimaterial bioink method for 3D printing tunable, cell-compatible hydrogels. Adv Mater 27:1607–1614. https://doi.org/10.1002/adma.201405076
Rutz AL, Lewis PL, Shah RN (2017) Toward next-generation bioinks: tuning material properties pre-and post-printing to optimize cell viability. MRS Bull 42:563–570. https://doi.org/10.1557/mrs.2017.162
Sun B, Hou Q, Liu Z, Ni Y (2015) Sodium periodate oxidation of cellulose nanocrystal and its application as a paper wet strength additive. Cellulose 22:1135–1146. https://doi.org/10.1007/s10570-015-0575-5
Sun H, Kim Y, Kim YC, Park IK, Suhr J, Byun D, Choi H, Kuk K, Baek OH, Jung Y (2018) Self-standing and shape-memorable UV-curing epoxy polymers for three-dimensional (3D) continuous-filament printing. J Mater Chem C 6:2996–3003. https://doi.org/10.1039/C7TC04873D
Yao C, Wang F, Cai Z, Wang X (2016) Aldehyde-functionalized porous nanocellulose for effective removal of heavy

metal ions from aqueous solutions. RSC Adv 6:92648–92654. https://doi.org/10.1039/C6RA20598D

Zhang B, Wang Q, Zhang Y, Gao W, Hou Y, Zhang G (2019) A self-assembled, nacre-mimetic, nano-laminar structure as a superior charge dissipation coating on insulators for HVDC gas-insulated systems. Nanoscale 11:18046–18051. https://doi.org/10.1039/C9NR06827A